ACS APPLIED MATERIALS & INTERFACES

Research Article

Cite This: ACS Appl. Mater. Interfaces 2019, 11, 7566−7575

www.acsami.org

Interlocked Graphene Oxide Provides Narrow Channels for Effective Water Desalination through Forward Osmosis

Nagarajan Padmavathy, Shasanka Sekhar Behera, Shabnam Pathan, Lopamudra Das Ghosh, and Suryasarathi Bose*

Department of Materials Engineering, Indian Institute of Science, Bangalore 560012, India

Supporting Information

ABSTRACT: Unique two-dimensional water channels formed by stacked graphene oxide (GO) sheets that are "nonleachable" and nonswellable can show great potential for water remediation. The interlayer spacing controls the solute or ion sieving and plays a crucial role in water transport in GO-based membranes. Herein, the sub-nano-channels adjacent to the sheets are altered by either ionic or covalent cross-linking using magnesium hydroxide ($Mg(OH)_2$) and graphene oxide quantum dots (GQDs) (named GOM and G-GQD), respectively. In aqueous solution, these cross-linkers prevent the GO sheets from swelling and precisely control the interlayer spacing required for water permeation. In addition, these narrowed GO sheets facilitate significant improvement in salt rejection of a divalent ion by forward osmosis and selective dye rejection and are resistive toward biofouling and bacterial growth. The cross-linked GO membranes are robust enough to withstand strong cross-flow velocity and aided in unimpeded water transport through the nanochannels. Among the membranes, the G-GQD membranes (G-GQD) show better antifouling characteristics, dye separation performance over 95−97% for various dyes, divalent ion rejection by 97%, and no cytotoxicity against HaCaT cells as compared with other GO membranes. Our findings on interlocking the domains of nanoslits of the GO structure by small ecofriendly molecules portray these materials as potential candidates for water separation applications.

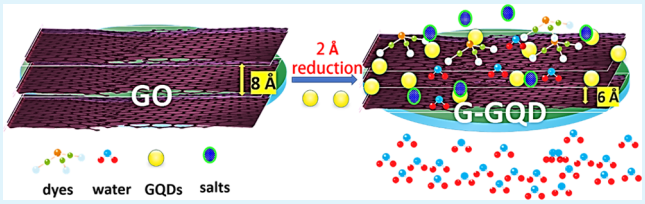

KEYWORDS: *graphene oxide, membrane, graphene oxide quantum dots, cross-linking, water treatment, forward osmosis*

1. INTRODUCTION

Increasing demand for quality water and scarcity of fresh water resources have impelled membrane technologists to develop energy-efficient, environmentally safe separation membranes.[1] Novel membrane materials with ease of synthesis are in great demand to meet the challenges of current reverse osmosis (RO) membranes. The unprecedented possibilities provided by the emerging two-dimensional layered materials, particularly, graphene oxide membranes, offer an extraordinary potential for separation applications.[2] GO has attracted a lot of attention for water transport studies because of its easy functionalization.[3,4] The pathway for water transport by GO membranes is formed between the nanochannels of GO sheets, which are swellable due to water intercalation, as has widely been reported.[5] This swelling can be minimized by a tailored approach via incorporation of charged functional moieties within the interlayer spacing of the flow channels like polyethyleneimine,[6] polyimidazole,[7] etc. as cross-linkers. Numerous efforts are being attempted to control the swelling of GO, mainly categorized into reduction[8,9] and cross-linking.[10] Nevertheless, the effectiveness of these strategies in tuning the interlayer spacing and a control over GO swelling in water still need further investigation.

The restacked GO membranes bound via $\pi-\pi$ interactions and hydrogen bonding give poor strength to the sheets; hence, delamination is obvious. Parallel diffusion of ions and molecules along the GO sheets within the network of interlayer channels is well established.[11] However, these ions can progressively diffuse through the adjacent GO sheet mediated via gap bridges; these defects in the form of cracks and holes help in separation of molecules and ions. Hence, connecting the sub-nano-channels by small molecules narrows the interlayer spacing, which is desired for preventing the delamination of GO sheets and for better separation performance of GO-based membranes.[12,13] The interlayer interaction between the GO sheets is primarily governed due to hydrogen bonding and weak van der Waals interactions. When these sheets stack together as a membrane, the interlayer interaction is weak and the disintegration becomes evident and unavoidable. To enhance the interlayer interaction, the only method that can be adopted is via chemical routes. In this work, two strategies are attempted to interlock the sub-nano-channels in GO, via ionic cross-linking with $Mg(OH)_2$ and covalent cross-linking with graphene oxide quantum dots (GQDs) by vacuum filtration on a polymeric support layer. The role of $Mg(OH)_2$ involves ionic cross-linking, wherein electrostatic attraction via ionic interaction is predominant in charged ions, forming Mg−O ionic bonds, providing excellent

Received: November 22, 2018
Accepted: January 25, 2019
Published: January 25, 2019

DOI: 10.1021/acsami.8b20598
ACS Appl. Mater. Interfaces 2019, 11, 7566−7575

stability to GO membranes.[14] The covalent cross-linking of GO sheets is achieved by GO quantum dots; abundant hydroxyl and carboxyl groups in GQDs make this system a versatile material for membrane applications.[15] Hence, to maintain the compatibility of GO sheets, GO quantum dots help in stitching the GO sheets by esterification, forming covalent cross-links for better stability of GO sheets.

The free-standing GO membranes thus obtained exhibited controlled water permeance and good efficiency in separation of dyes and salts and provided excellent stability due to precisely controlled interlayer distance by rigid short bonds. The G-GQD membrane demonstrated significant improvement in salt rejection, antibiofouling performances, and antibacterial characteristics comparable to those of pristine GO membranes. The smaller-sized GQDs do create more sub-nano-channels, can bind with GO through hydrogen bonding, and may lead to interlocked structures, which can sieve organic molecules, dyes, ions, etc. The cytotoxicity assay of the permeate against HaCaT cells revealed that the G-GQD membranes have enhanced biocompatibility than that of GO and GOM membranes.

2. EXPERIMENTAL SECTION

2.1. Materials. Magnesium nitrate of >98% purity ($Mg(NO_3)_2$), hydrogen peroxide (H_2O_2), sodium hydroxide of 99% purity (NaOH), hydrochloric acid (HCl), sulfuric acid (H_2SO_4), phosphoric acid (H_3PO_4), dicyclohexylcarbodiimide (DCC), sodium sulfate (Na_2SO_4), 4-dimethylaminopyridine (DMAP), potassium permanganate ($KMnO_4$), methanol, methyl orange (MO), methyl red (MR), and methylene blue (MB) have been procured from Sd Fine Chem Private Limited. Graphite powder is obtained from Superior Company, India. Hydrophilic poly(vinylidene difluoride) (PVDF) membrane (0.125 μm, 47 mm), bovine serum albumin (BSA), and dichlorofluorescin diacetate (DCFH-DA) dye are procured from Sigma-Aldrich.

2.1.1. GO Synthesis. Modified Hummer's method is adopted for the synthesis of GO, as reported elsewhere.[16] Briefly, graphite powder (1 g) is introduced to a mixture of H_2SO_4 and H_3PO_4 (62 mL and 55:7 by volume) and mechanically stirred for 30 min at 0−4 °C. $KMnO_4$ (6 g) is added to the aforesaid mixture, and stirring is continued at 25 °C for 3 days for complete oxidation. To arrest the reaction, H_2O_2 is added dropwise and excessive $KMnO_4$ is neutralized. The formed graphitic oxide is washed thoroughly with 1 M HCl and deionized (DI) water. The obtained GO is centrifuged and dried in vacuum for further use.

2.1.2. $Mg(OH)_2$ Synthesis. $Mg(OH)_2$ is synthesized by the hydrothermal process.[17] In brief, 1 M $Mg(NO_3)_2$ and 2 M NaOH are dissolved in 100 mL of DI water. The solution is then stirred for 15 min and kept in a Teflon-lined autoclave at 180 °C for 24 h. Afterward, the centrifugation process is carried out by washing with DI water several times followed by ethanol until the pH becomes neutral. The as-prepared $Mg(OH)_2$ powder is dried at 60 °C for 12 h under vacuum (detailed characterization is given in Figures S1 and S2).

2.1.3. GQD Synthesis. GQDs are synthesized according to the procedure reported earlier.[18] Briefly, 20 mL of 30% H_2O_2 is added to 100 mg of GO and sonicated for 5 min. Then, the thoroughly mixed reactants are kept for hydrothermal synthesis in the autoclave at 180 °C for 2 h. Then, the reaction mixture is centrifuged at 7000 rpm and washed 5−6 times with DI water till pH 6 is reached (detailed characterization is given in Figures S3 and S4).

2.1.4. Synthesis of GO-g-GQDs. The covalent functionalization of GQDs with GO is done by the Steglich esterification reaction.[19] Typically, 30 mg of GO and 70 mg of GQDs are suspended in 20 mL of tetrahydrofuran (THF). The suspension is stirred at 25 °C for 1 h, and subsequently, DCC (5 mmol) and DMAP (1 mmol) are added in THF. The resulting mixture is stirred at 25 °C for 24 h. The solid product is centrifuged and dried at 50 °C under vacuum.

2.1.5. Fabrication of GO and Modified GO Membranes. The pristine GO membrane is prepared by depositing the suspension of 0.5 mg/mL concentration onto a hydrophilic PVDF membrane through vacuum-assisted filtration. The alignment of GO nanosheets can be promoted by very slow filtration speed (~0.1 mL/min). The obtained GO membrane is vacuum-dried at 40 °C for 8 h. To prepare an ionically cross-linked GO membrane, the as-prepared $Mg(OH)_2$ powder is added with GO (2:3 ratio by wt %) and the total concentration of the suspension is maintained at 0.5 mg/mL, followed by vacuum filtration on the polymeric support. Likewise, the cross-linked GO-*g*-GQDs of 0.5 mg/mL suspension are made as a membrane. Eventually, the three membranes obtained, named GO, GOM, and G-GQD, represent pristine, ionically cross-linked, and covalently cross-linked membranes, respectively.

2.2. Characterization. A mid-infrared spectrometer (FT-IR) by PerkinElmer Frontier (4000−650 cm^{-1}) is used to characterize all of the GO membranes. AXIS Ultra X-ray photoelectron spectroscopy (XPS) is adopted for the elemental analysis of the GO membranes. The GO morphologies in the dispersed state are carefully evaluated by transmission electron microscopy (TEM, FEI Technai G^2). For this, a particle dispersion drop is mounted on a 200-mesh copper grid. The roughness of the exfoliated GO is obtained by atomic force microscopy (AFM, Bruker, Dimension ICON). The cross-sectional observation of cryofractured GO membranes in liquid nitrogen is done by ULTRA 55 Carl Zeiss scanning electron microscopy (SEM). The interlayer spacing of wet and dry GO membranes is obtained using PANalytical X'pert PRO for X-ray diffraction (XRD) studies. For wet membrane studies, a drop of petroleum ether is added on the dried membranes after immersing 24 h in water. The ζ-potentials of GO dispersions and solid membranes are determined using a ζ-potential analyzer (Zetasizer NanoZS90, Malvern Instruments) and an electro-kinetic analyzer, SurPASS, Anton Par, respectively.

The sessile drop contact angle of the GO dispersions is measured at 25 °C with relative humidity 60% with 3 μL droplets using FTÅ 200, Dataphysics. Triplicates of each observation are made in different locations to assess water droplet stability.

2.2.1. Flux and Rejection Measurements. Water permeation and salt rejection are performed by sealing the respective membranes on PVDF separately with O-rings in an inbuilt forward osmosis (FO) setup (Figure S5). The feed and draw are maintained at room temperature, and the system is operated at a cross-flow rate of 400 mL/min and a maximum pressure of 10−30 psi. Feed and draw solutions are drawn in triplicate. The Na_2SO_4 solution (2000 ppm) acted as the draw solution, whereas DI is the feed. The water flux (J_w), reverse solute flux (J_s), and salt rejection (R) are determined by the volume changes of the feed and draw solutions at predicted intervals up to 24 h. J_w and R are computed using the following equations.[20]

$$J_w = \Delta V/A{\cdot}\Delta t$$

where ΔV is the change in volume of feed on time lapse Δt with A as the effective area.

Salt rejection

$$R = [1 - (C_{ft} - C_{fo})/C_{do}] \times 100$$

where C_{ft} and C_{fo} are the final and initial feed concentrations and C_{do} is the initial concentration of draw.

2.2.2. Antifouling Measurements. The antifouling properties of GO, GOM, and G-GQDs membranes are assessed by the dynamic adsorption fouling test taking BSA model protein using the reverse osmosis setup. The active layer maintained is GO with PVDF as the base. BSA is passed along the cross-flow setup (0.3 g/L, pH 7.4) at different pressures. The membranes are then dipped in phosphate buffer solution and are tested in trplicate.

Based on these results, the recovery of these membranes is evaluated using the flux recovery ratio (FRR), the flux decline is monitored using the irreversible flux decline ratio (IFR), and the antifouling ability is evaluated using the relative fouled flux ratio

DOI: 10.1021/acsami.8b20598
ACS Appl. Mater. Interfaces 2019, 11, 7566−7575

Scheme 1. (a) Fabrication of GO, GOM, and G-GQD by Vacuum-Assisted Filtration Using a Porous Polymeric Support and (b) Formation of GO-Based Membranes and Their Corresponding Structures

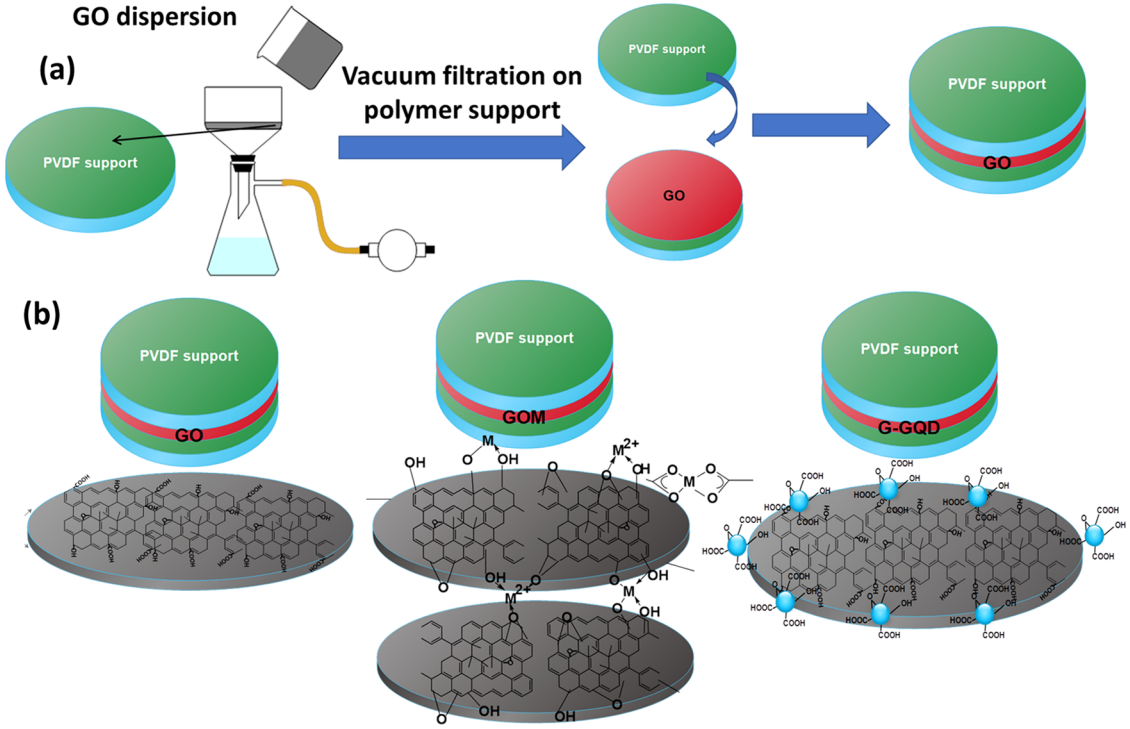

(RFR). It is well documented in the literature that higher FRR and significantly lower IFR attribute to better antifouling properties.

Precisely, to obtain the results, the filtration process is executed in three steps, namely, stable flux (J) via water filtration, followed by charged pollutant feed (BSA) and subsequently by another stable flux (J_P). The cleaning process is performed on the GO membrane by a gentle phosphate buffer for 10 min followed by rinsing. The calculations of FRR, IFR, and RFR are stated below.

$$\text{FRR} = J_2/J \times 100\% \quad (1)$$

$$\text{IFR} = (1 - J_2/J) \times 100\% \quad (2)$$

$$\text{RFR} = J_p/J \quad (3)$$

2.2.3. Dye Rejection Studies. The dye rejection experiments are performed using GO, GOM, and G-GQD membranes on the cross-flow setup. The stock solutions of 100 ppm MO, MR, and MB dyes are prepared, diluted to 10 ppm, and maintained throughout the experiment. Rejection is calculated by subtracting the original amount in the feed solution from the amount of the dye in permeate using $[1 - (C_{permeate} - C_{feed}) \times 100]$, where C is the dye concentration. The rejection experiments are carried out at 1−2 bar, and the feed and permeate concentrations are monitored by UV−visible spectroscopy (PerkinElmer) between 200 and 800 nm. All of the three GO membranes are tested as described above.

2.2.4. Biological Studies. 2.2.4.1. Bacterial Culture. The antibacterial studies are carried out using *Escherichia coli* (MG 1655) obtained from NCBS, Bangalore. The strain is subcultured at 37 °C from a revived master stock on freshly prepared Luria-Bertani broth. From this, a new subculture is obtained and normalized at an O.D. of 0.8. The supplemented bacteria are then made devoid of media by centrifuging them to obtain bacterial pellets, which are then rinsed with PBS three times before resuspending again in the PBS.

The *E. coli* culture (100 μL) is then introduced to 96-well plates containing different GO-based membranes and incubated in a shaking incubator for 4 h. A 5-fold serial dilution is performed using the spreader technique to obtain plate count results. These plates are incubated in an incubator at 37 °C for 24 h.

2.2.4.2. Analysis of Reactive Oxygen Species (ROS). The ROS produced by these membranes (GO, GOM, and G-GQD) is examined using the dichlorofluorescin diacetate dye. The dye is added to the bacterial suspension and incubated for 30 min in the dark. The fluorescent measurements are performed by exciting at 485 nm and collecting emission signals at 528 nm. All of the GO membranes in PBS are evaluated, and the bacterial suspension in PBS is used as a control.

2.2.4.3. Cytotoxicity Studies. The cytotoxicity of GO and modified GO membranes is evaluated for cell viability and proliferation of HaCaT cells using the permeates collected from the membranes after 24 h by quantifying the DNA content at days 1, 3, and 5 using the Picogreen assay (Life Technologies). The collected permeate is sterilized using a 0.22 μm membrane prior to cell culture. The sterile permeate is added to the culture media at a ratio of 1:1 and used for seeding and culturing of the cells for 5 days. Initially, 1×10^4 cells are seeded per well of 24-well plates. DNA quantification is done as per our previous report.[21] The DNA content of permeates is calculated using the standard plot.

Cell viability is also assessed microscopically using the live/dead staining kit from Life Technologies and performed at days 1, 3, and 5 post seeding. The live cells are stained with calcein AM, whereas ethidium bromide stained the dead cells. Using an Olympus IX epifluorescence microscope, cells are imaged[16] at 488 and 594 nm for live and dead cells respectively. One-way variance analysis is performed between the groups to obtain the statistical difference with p values ≤0.05.

3. RESULTS

3.1. Fabrication and Characterization of GO Membranes. The choice of the membrane support determines the adhesive nature of GO sheets. Thus, in this study, using hydrophilic porous PVDF as a support layer, the GO membranes are deposited through vacuum filtration (see Scheme 1a). Stable free-standing membranes with $Mg(OH)_2$ (Scheme 1b) and GQDs (Scheme 1b) are obtained. Alkaline earth metal salts like $MgCl_2$ and $CaCl_2$ are known to bind to

DOI: 10.1021/acsami.8b20598
ACS Appl. Mater. Interfaces 2019, 11, 7566−7575

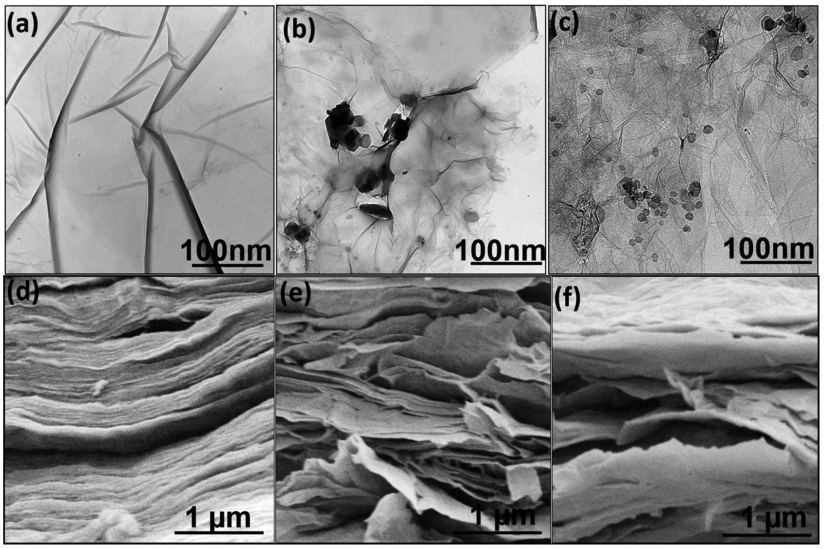

Figure 1. Surface morphology of GO, GOM, and GQD membranes: TEM images of fine dispersions of (a) GO (b) GOM, and (c) G-GQD. Cryofractured cross-sectional field emission SEM images of (d) GO (e) GOM, and (f) G-GQD membranes.

the oxygen functionalities as cross-linkers.[22] The chloride salts tend to agglomerate GO sheets immediately due to cross-linking by divalent ions. Thus, we employed $Mg(OH)_2$ to pristine GO (Figure 1a) and no such aggregation is seen (Figure 1b) presumably because OH^- ions form intermolecular hydrogen bonds with functional groups of GO, which minimize the unbound or weakly bound metal ions among the GO sheets[23] (Scheme 1b).

GO quantum dots can function as nanocapillaries and enhance the dispersibility of the GO membrane. GQDs maintain the same thickness as of GO but possess a diameter of 5−20 nm[24] (Figure S4). The nanoparticles with key functional groups (GO quantum dots) help in stitching the edges of GO sheets by covalent cross-linked structures. It provides a dense structure between the GO layers and hence narrowing the interlayer spacing by simultaneously improving the capillary interaction. The removal of charged oxygenated functional groups of GO during esterification with GO quantum dots presumably enhances the $\pi-\pi$ interaction, thereby controlling the interlayer spacing.

3.2. Effectiveness of Cross-Linking. The role of cross-linking is to enhance the stability of GO sheets when exposed to aqueous medium. Mg ion-intercalated GO membranes showed an increased interlayer spacing (9.9 Å, Figure 2a) compared to that of the unmodified GO membrane (8 Å, Figure 2a). It must be noted here that the 2θ value of native GO of 10.8° has shifted to lower values in the case of GOM to 8.5°, suggesting the intercalation of the Mg^{2+} ions with GO. The characteristic peaks of $Mg(OH)_2$ are observed in GOM along with GO, which suggests that Mg^{2+} with an ionic radius of 0.78 Å can easily intercalate into the basal planes of GO.[25]

In the case of the G-GQD membrane, the characteristic peak of GQD at $2\theta = 25.5°$ corresponds to the (002) plane, whereas the GO peak is shifted to higher 2θ from 10.8 to 14.1°, clearly illustrating the interlayer spacing of 6.1 Å (Figure 2a), which is lower than that of pristine GO. These data suggest that the oxygenated functional groups reacted with GO functionalities by esterification and are interconnected within sub-nano-channels of GO, thus narrowing the interlayer spacing (from 8.2 to 6.1 Å) (Table S1). We further analyzed the narrowing of *d*-spacing with AFM measurements. From AFM analysis, the thicknesses of monolayers of GO and G-GQD are 1.03 and 0.85 nm, respectively. Although the reduction in thickness is not exactly matching with diffraction data but is in agreement with the XRD result. The height profile of G-GQD exhibits a smooth surface with a roughness of 1.36 nm, whereas GO shows an average roughness of 5.97 nm. These semi-quantitative AFM results lead to narrowed interlayer spacing of GO in G-GQD (Figure S6). It is interesting to note that these modified GO membranes behave differently in water; the interlayer spacing significantly altered based on the nature of bond formation when compared with native GO (Table 1). The free permeance of water molecules between the layers of wet GOM enlarged the *d*-spacing (Table 1). However, the G-GQD membrane did not swell after immersing for 24 h in water, which is manifested from its unaltered *d*-spacing of 6 Å (Table 1).

FT-IR analysis reveals that as compared to GO, GOM exhibits a decrease in C−O stretching intensity besides the peak position shifting to lower wavenumbers. This is attributed to the ability of coordination of divalent ions to the carboxylic acid groups of GO in GOM (Figure 2b). In G-GQD, two new peaks at 1020 and 1715 cm^{-1} corresponding to −C−O−C and −C═O of an ester group (−O−C═O) appear, thus confirming the covalent bond formation between GO and GQDs (Figure 2b). This is further supported by XPS characterization (Figure 2c).

The XPS data (Figure 2c) of GO membranes showed that unoxidized carbon content, oxygen functional groups, and the oxidized functional groups on the GO membranes could readily react with Mg^{2+} ions. In GOM, it is clearly envisaged that the decrease in oxygen content indicates the formation of metal chelates with $Mg(OH)_2$. In the case of GOM, the existence of the Mg 2p peak at 48.8 eV, with a wide hump, indicates the Mg−O ionic bond (Figure 2c inset). It is envisaged that the interlinkage of Mg^{2+} and GO stems from the chelation of C−O−C with Mg, leading to the Mg−O ionic bond, serving as interlayer cross-links. It might be ascribed to the fact that the carboxylates, COO^-, of two adjacent GO sheets bridge Mg^{2+}, leading to intercalated Mg−GO chelates.

This is reflected in the ζ-potential values of GOM and the increase in the surface charge of the GO modified membrane

DOI: 10.1021/acsami.8b20598
ACS Appl. Mater. Interfaces 2019, 11, 7566−7575

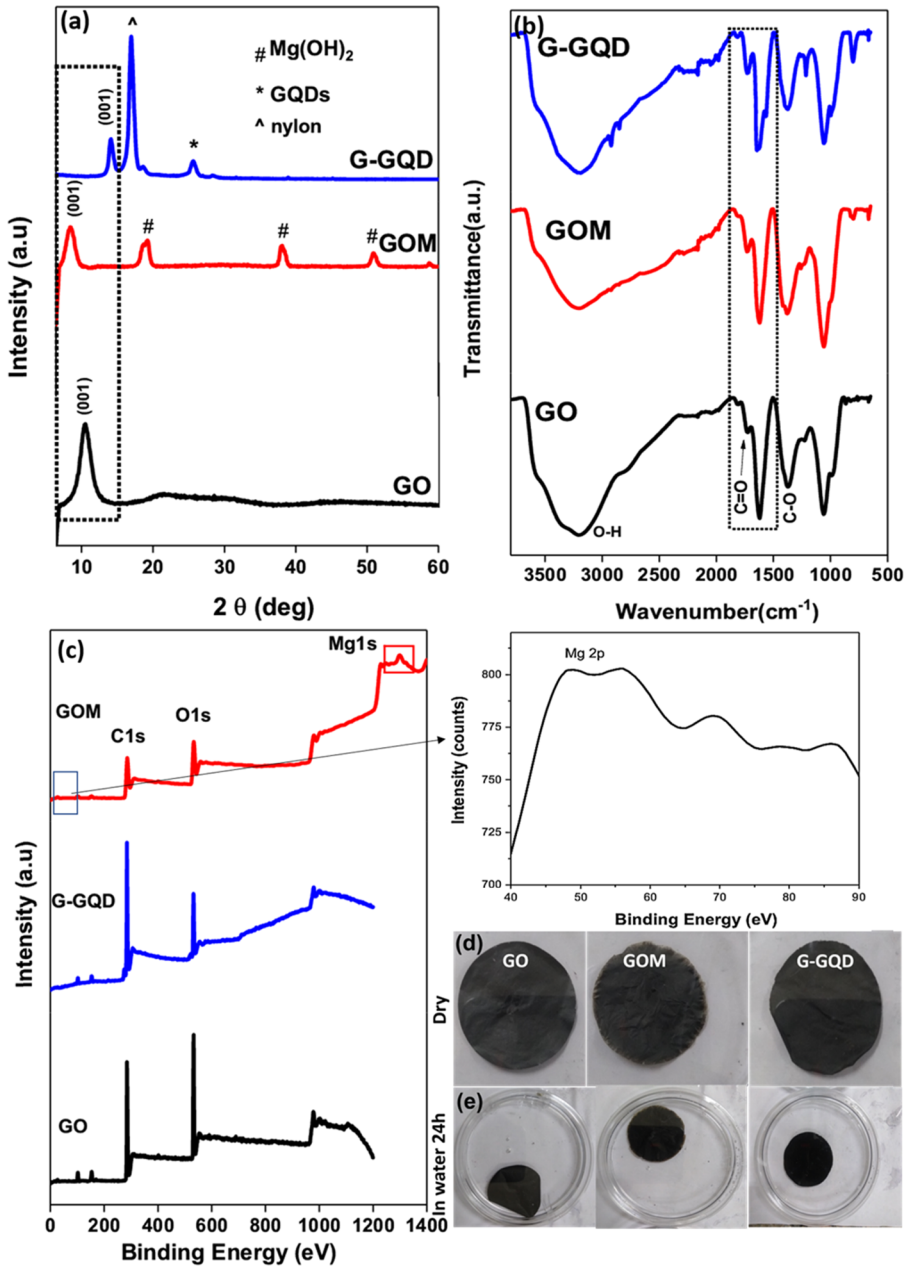

Figure 2. Characterization of GO, GOM, and G-GQD membranes: (a) XRD spectra indicate the interlayer spacing, (b) FT-IR spectra, (c) XPS survey spectra, and the enlarged view of Mg 2p in GOM, and (d, e) photographs of GO, GOM, and G-GQD in dry and wet conditions, respectively.

Table 1. Interlayer Spacings in Dry as well as in Wet Conditions[a]

		d-spacing (Å)		ζ-potential (mV)	
				dispersion	membranes
membranes	immersion time in water (h)	dry	wet	wet	dry
GO	24	8	12.6	−16.1	−8.6
GOM	24	9.9	13.5	−12.8	−13.1
G-GQD	24	6	6	−28.6	−14.0

[a]ζ-Potential of GO dispersions at pH 6.8 and of GO membranes at pH 6.7.

(Table 1). The G-GQD membrane showed almost equal contents of carbon and oxygen elements, which is ascribed to the strong cross-linking between GO and GQDs by the esterification reaction. By immersing the GO-based membranes in water for 24 h, no visual delamination was found for GO sheets, which showed that the membranes are quite stable (Figure 2d,e). From the above detailed characterization of the GO, GOM, and G-GQD membranes, the cross-linking assists the membranes in keeping their integrity in water for several days without any disintegration. Furthermore, the water transport, desalination, and separation of dyes by GO membranes are systematically performed in detail.

3.3. Water Transport Properties. Ideally, optimum filtration performance can be achieved when a membrane is as thin as possible, as selective as possible, and as robust as

DOI: 10.1021/acsami.8b20598
ACS Appl. Mater. Interfaces 2019, 11, 7566−7575

possible. The cross-linking in GOM and G-GQD as discussed above enables us to test the permeation of water and separation properties. We tested water permeation, salt and dye rejections, and antifouling performance of pr GO membranes.

The water flux of GO increased from ca. 95 LMH to ca. 110 LMH for GOM, and for G-GQD, it is measured as ca. 55 LMH after 24 h (Figure 3a). This clearly shows that the role of

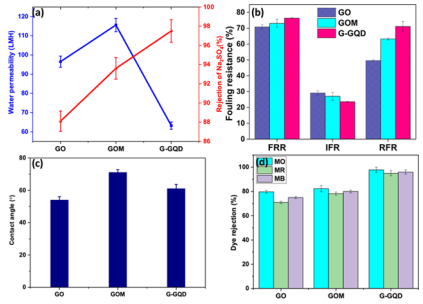

Figure 3. Water transport properties of GO, GOM, and G-GQD membranes. (a) Flux study of water permeance and the salt rejection of Na_2SO_4 tested in the FO system as a feed and under 1−2 bar for 24 h. (b) Antifouling studies at 30 psi, (c) contact angle measurements for hydrophilic nature of membranes, and (d) dye rejection performances of MO, MR, and MB.

interlayer spacing in each GO membrane is because of not only the omission of the PVDF support layer but also the low friction of the enlarged gap as nanochannels. G-GQD has shown water flux lower than that of its counter membranes, indicating the tightened interlayer spacing by GQDs. The water flux of the GO-based membranes is studied for 21 days. The results manifested clearly that all of the GO membranes showed reduction in water permeability to 3−4 LMH at constant 30 psi pressure. Between days 1 and 21, a substantial decrease is noted for all of the membranes, which can be attributed to the compaction of GO membranes by forming wrinkles, which led to a decline in the flux. Furthermore, the stability of the GO-based membranes up to 45 days is tested by immersing GO membranes in water. GO disintegrated quickly in water within few days, but modified GOM and G-GQD membranes were stable up to 45 days. Mg ions and GO quantum dots enhance interfacial compatibility between GO sheets by effective cross-linking (Figure S7).

3.4. Effect of Narrow Spacing: Desalination Performance by FO. The effectiveness of cross-linking in GO membranes can be understood by transport properties of the membrane. Using Na_2SO_4 as a model divalent salt, the salt rejection by the pristine GO, GOM, and G-GQD membranes is tested (Figure 3a). Under the reverse osmosis cross-flow setup, the pressure is increased slowly from 10 to 60 psi, and the GO membranes disintegrated under high pressure, so further the salt desalination experiment could not be performed. Then, using the pressure-driven forward osmosis setup, a Na_2SO_4 solution is chosen as a draw solution at a higher concentration (2000 ppm), whereas DI water acted as the feed. A maximum pressure of 30 psi is applied to the feed side, whereas the draw side is left at its own disposal. The pressure is not increased beyond 30 psi because FO membranes perform on the basis of an osmotic pressure gradient. Over time (24 h), GO-based membranes showed a similar trend of salt rejection at 10, 20, and 30 psi. No significant difference is observed (Figure S8).

The salt rejection is wholly contributed by GO since the PVDF support alone imparted nothing. The GO membrane displayed 85% rejection, but G-GQD showed 97% rejection of Na_2SO_4, which can likely be ascribed to the fact that covalently interlocked GQDs to GO narrowed the interlayer spacing and prevented the membrane from swelling. Interestingly, GOM exhibited high rejection (95%) compared with GO membranes. This can be attributed to the partial counter rejection of cations (Na^+) on the surface of GOM.

3.5. Antifouling Studies. Fouling resistance is dependent on the hydrophilic surface, which is mediated by suppressing the nonspecific interactions and preventing the foulants from attaching onto the surface of the membrane. GO-based membranes are inherently hydrophilic and show better antifouling characteristics.

The fouling tests are performed against BSA at 30 psi by measuring the initial stable water flux followed by the addition of BSA, which showed decreased fluxes. Subsequently, the recovered fluxes are measured when the fouled membranes are washed with PBS. The results of the fouling tests indicated that the insertion of $Mg(OH)_2$ did not significantly improve the fouling resistance of the GO membrane. This is clear that natural organic matter acts as a coordination donor for metal ions like Ca^{2+} and Mg^{2+} to form complexes.[26] In our case, GOM primarily coordinated with GO functional groups (Scheme 1b); hence, the flux recovery ratio (FRR) is only 73% (Figure 3b). At the same time, the G-GQD membrane showed a higher recovery ratio of 77% as compared to that of GO (70%) and a higher fouling resistance against BSA. The total fouling rate of G-GQD is 22%, which is better than that of GO (30%) and GOM (27%). The improved antifouling properties of the GO membranes resulted from the increase in surface hydrophilicity by incorporating GQDs into GO (Figure 3c). The adsorption of foulants on the GO membrane surface is reduced due to surface hydrophilicity of GQDs, and this promoted desorption of hydrophobic foulants from the GO surface. Moreover, BSA contains negative charges at neutral pH and the electrostatic repulsion is experienced more by G-GQD possessing a more negative surface than by GO and GOM both in solution and as thin membranes (Table 1).

3.6. Dye Rejection Studies. The dye rejection by the GO-based membranes has been evaluated using MO, MR, and MB as model azo dyes, which diffuse in water as contaminants. Many organic dyes are adsorbed on GO based on the superficial charge. MO is an anionic dye, and it can be expected that charge repulsion may occur between GO-based membranes and MO.[27] It is understood from our studies that all of the GO membranes showed great permeability and better separation efficiency of the dyes. GO membranes exhibited 82.5 ± 1%, GOM showed 87.7 ± 1%, and G-GQD displayed 97 ± 2% rejection (Figure 3d). A similar trend is noted for other dyes too. G-GQD rejected almost all of the dyes (>95%) as compared with GOM and pristine GO. Since the modified GO membranes are negatively charged at neutral pH, it is expected that the anionic dye MO can easily be rejected by the membranes via electrostatic repulsions. However, cationic dyes are being adsorbed at the nanochannels that could be partially blocked at the membrane surface, resulting in a decrease in flux. We checked this possibility when the feed concentration of dye is 10 times (100 ppm) higher than that of the tested solution; the saturation of separation of dyes is reached. To

DOI: 10.1021/acsami.8b20598
ACS Appl. Mater. Interfaces 2019, 11, 7566−7575

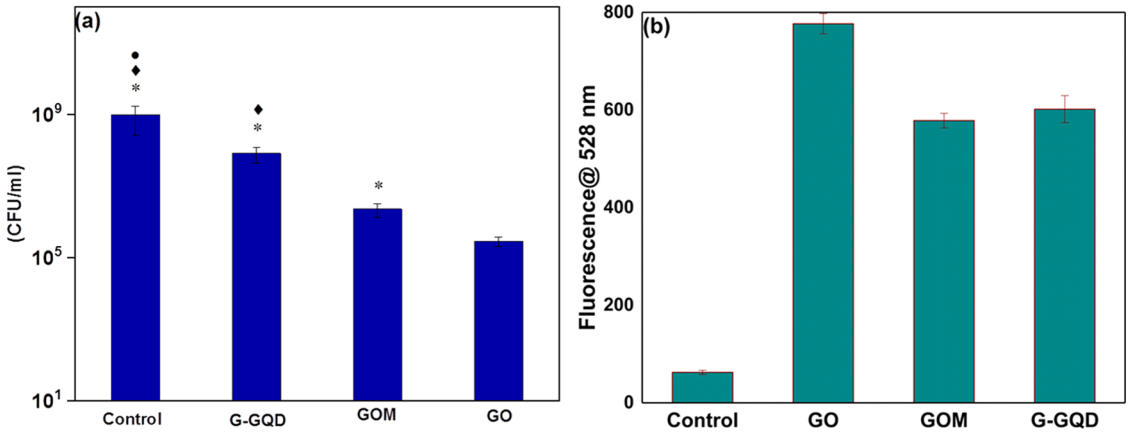

Figure 4. (a) Antibacterial activity of GO, GOM, and G-GQD membranes. For the antibacterial assay, bacterial cells are kept in contact with the membranes for 4 h. (b) ROS production from the permeate of the membranes measured at an emission wavelength of 528 nm. Significant statistical differences ($p < 0.05$) compared with control for G-GQD, GOM, and GO are indicated by *, ◆, and ●, respectively.

evaluate the rejection efficiency, we monitored the UV−vis spectra of the permeate to get a telltale signature of methyl orange. The absorption peak centered at 463 nm is attributed to MO, which decreased dramatically for all of the GO membranes for G-GQD (Figure S9). These results indicate that G-GQD membranes can have great potential in water remediation. A similar trend is noted for methyl red and methylene blue too (Figure 3d). The water flux of all of the membranes tested at the RO system cross-flow setup is shown in Figure S10.

3.7. Biological Properties. *3.7.1. Antibacterial Assessment.* The modified GO with enhanced functional groups may contribute significantly toward antibacterial activity. The intercalation of $Mg(OH)_2$ and GQDs offers abundant functionalities and are expected to give enhanced antibacterial properties. Using *E. coli* as a model system, 10^7 CFU/mL cells are incubated along with the membranes in PBS solution for 4 h. The ability of GO membranes to be a biocide is assessed by the plate counting method.

Figures 4a and 5 show the bacterial viability after 4 h of contact time, where the GO membrane showed better

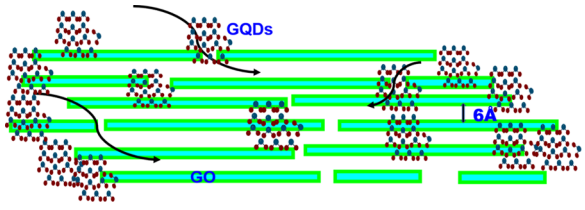

Figure 5. Schematic illustration of the narrowed interlayer spacing of the GO membrane by GQDs to 6 Å, indicating the effective separation of salts, dyes, etc.

reduction of bacterial colonies, whereas GOM and G-GQD membranes expressed minimal bacterial killing of 1.1 log and 0.7 log reduction, respectively. It can be evidently stated that more than 90% of the bacteria are inactivated by all of the GO membranes. It is expected that GOM would show better antibacterial characteristics than those of GO and G-GQD as $Mg(OH)_2$ is a potential antibacterial agent[28] besides acting as a cross-linker in this study. However, the complexation of $Mg(OH)_2$ with GO functionalities showed minimal bactericidal properties against intracellular bacteria as compared to those of GO and G-GQD.

The antibacterial action of GO as a flat surface and as dispersions against different bacterial strains and its mechanism have been extensively reported.[29] In addition, the lateral dimension of GO is also to be considered with an alteration in the antibacterial activity when the size is down to nanometers.[30] GQDs, which are 5−20 nm in size, exhibited minimum reduction in cell viability in both the dry and suspension modes; it is speculated that GQDs enwrap the bacterial cells with no sharp edges. In previous studies, the flat graphene oxide sheets induced membrane stress by direct physical interaction and oxidative stress, which is mediated by membrane puncturing through sharp edges of graphene domains.[31] Conclusively, the capability of killing bacterial cells is minimum for G-GQD followed by GOM and GO. Hence, we assessed the reactive oxygen species assay to quantify the GOM and GQD membranes in suspension for identifying a reversible cell entrapment mechanism.[32]

3.7.2. ROS. To critically assess the manifestation of intracellular ROS, 2′,7′-dichlorofluorescin diacetate (DCFH-DA) is used as a visual indicator. DCFH-DA is permeable to microbial cells and hydrolyzes in the presence of intracellular esterase to nonfluorescent DCFH. In the presence of upscaled intracellular stresses, oxidation of DCFH occurs, leading to the formation of highly fluorescent dichlorofluorescein. The extent of this fluorescence is directly proportional to the intracellular stress by oxidative species.[33] Figure 4b illustrates the ROS generation in GO, GOM, and G-GQD in the presence of DCFH. This revealed an increase in fluorescence intensity (ca. 3.5-fold) for pristine GO membranes compared to that for cross-linked GOM and G-GQD membranes. In the literature, no superoxide radical anion-induced ROS is observed, but still the oxidative stress of GO can be caused by bacterial deposits on the GO material mediated via direct contact with sharp nanosheets.[34]

These results suggest a possibility of aggregation of GQDs within GO sheets, yielding the antimicrobial activity, and bacterial resistance showed no significant enhancement than that in GO. Nevertheless, GOM and G-GQD membranes showed minimum toxicity against bacteria and behave as bacteriostatic membranes.

DOI: 10.1021/acsami.8b20598
ACS Appl. Mater. Interfaces 2019, 11, 7566−7575

4. DISCUSSION

A GO sheet contains 82% oxidized part, 16% nonoxidized domains, and 2% holes.[35] Herein, we establish stable GO-based membranes using oxidized domains for controlled permeability of water and good separation efficiency by intercalating $Mg(OH)_2$ and "interlocking" GQDs. It is found that $Mg(OH)_2$ and GQDs prevent delamination of GO sheets, efficiently cross-link the GO sheets, enlarge/narrow the interlayer distance between GO sheets, and reject organic dye molecules. These membranes show water permeance over 90−95 LMH and are scalable at industrial levels.

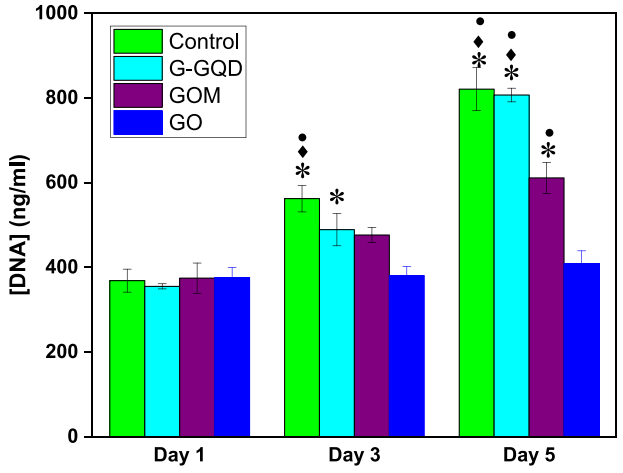

Figure 6. Picogreen assay conducted with the permeate collected from GO, GOM, and G-GQD after 24 h. Fluorescence is measured at excitation and emission of 485 and 528 nm, respectively. Significant statistical differences ($p < 0.05$) compared to control for G-GQD, GOM, and GO are indicated by *, ◆, and ●, respectively.

As oxygenated functional moieties are prone to corrugate the GO sheets, the cationic modification (Mg^{2+} ions) and GQDs prevent such clustering, leading to specific percolating regions in nonoxidized graphene. Pristine nanochannels are formed as a result of vacant regions of nonoxidized graphene sheets.[36] We have utilized these empty spaces between the oxidized parts by intercalating $Mg(OH)_2$ and GQDs. Mg ions form intercalates at the edges (Scheme 1b), but GQDs occupy these spaces (Figure 6). However, the simple esterification reaction assisted in stitching the GO sheets at the edges by GQDs to connect the neighboring GO, resulting in narrowing of interlayer spacing (Figure S11). The existence of oxidized and nonoxidized domains primarily governs the interlayer spacing of the GO sheets and greatly influences the ion and molecule diffusivity (Figure S12).

Most of the modified GO membranes demonstrate the separation efficiency >95% by incorporating larger charged organic moieties.[37] In a longer run, these molecules would lead to instability, resulting in adverse effects. $Mg(OH)_2$ and GQDs are relatively safe materials at a lower dosage, and leaching from the GO sheets is completely minimized by ionic and covalent cross-linking. The very next uncertainty is whether these GOM and G-GQDs membranes would leach when they are in use for longer time points. Hence, we performed the cytotoxicity studies against HaCaT cells with the permeate collected after 24 h from each GO, GOM, and G-GQD membrane. From Figure 6, it is obvious that the GO modified membranes showed no observable cytotoxicity with HaCaT cells up to 5 days. The G-GQD membrane is expected to be nonleaching and exhibited enhanced cell proliferation even at the fifth day.

GO has a potential cytotoxic effect on human cell lines; however, in the present case, G-GQD and GOM completely "stitched" the GO sheets and hence leaching of GO in the permeate is greatly reduced. As evident from Figure 7, the cells are live and proliferating even after 5 days, thereby suggesting that the permeate is noncytotoxic, which is in sharp contrast to the GO membrane, which is found to be toxic.

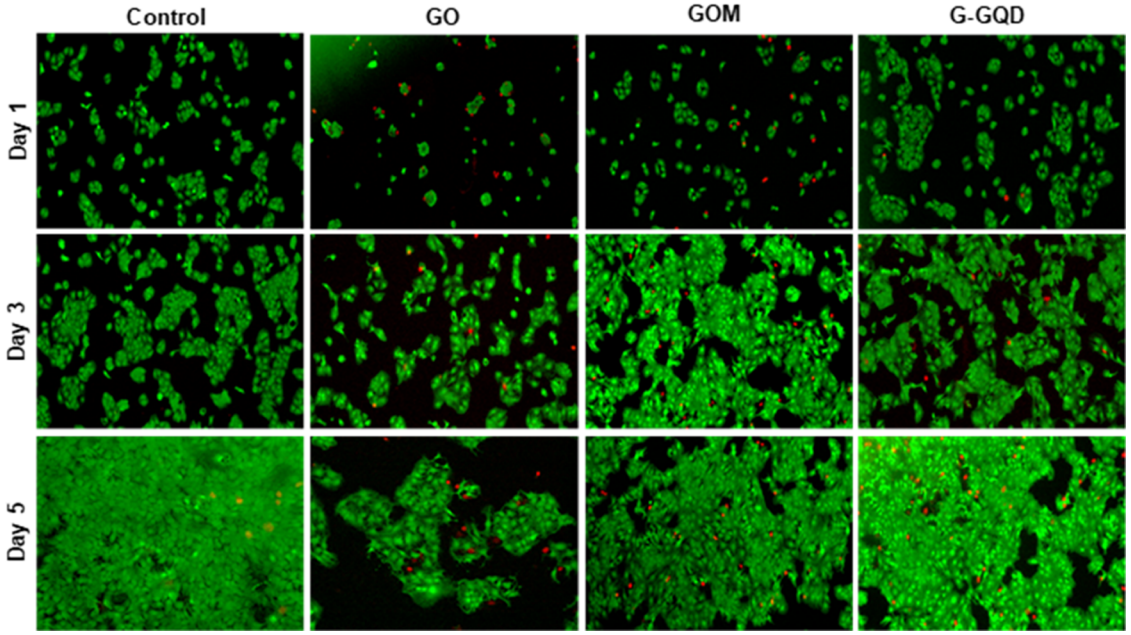

Figure 7. Representative fluorescent micrographs showing live cells stained with calcein AM (green) and dead cells stained red with ethidium bromide on culturing with permeates of each GO membrane at days 1, 3, and 5.

DOI: 10.1021/acsami.8b20598
ACS Appl. Mater. Interfaces 2019, 11, 7566−7575

Proliferation of HaCaT cells is observed in our case (up to 5 days) on treatment, even though bare micron-sized GO is reportedly claimed as a cytotoxic material,[38] and the edge effect of GO is greatly minimized by the biocompatible GQDs against the normal cells and tissues.[39] The live/dead staining further corroborates these results (Figure 7) and also proves the cytocompatibility of the G-GQD membrane over that of GO and GOM membranes.

The interplanar gaps are narrowed with GQDs by covalent bonds and with native coordination complexes by Mg^{2+} ions via ionic cross-linking. Hence, these modified GO membranes are safe and resulted in flux and desalination comparable to those of existing RO membranes and rejection of dyes comparable to that of modified GO membranes.

5. CONCLUSIONS

In this work, we fabricated robust GO membranes with narrowed spacing for separation of small dye molecules and divalent ions by forward osmosis. The developed approach is a facile and practicable method of chemically decreasing the interlayer spacing and controlled swelling by interlocked GO sheets. The GQD-modified GO membranes showed a high permeability for water 30-times more than that of the RO membrane, better antifouling behavior, and moderate antibacterial properties than those of GO and GOM. As an effort of narrowing of interlayer spacing of the G-GQD membrane to 6 Å, improving the rejection of divalent salt rejection to 97% and various dyes up to 95%. The noncytotoxic characteristics exhibited by modified GO membranes against HaCaT cells indicate the effectiveness of covalent cross-linking. Our study can be a platform for highly versatile separation of dyes, ions, and even solvent molecules through environmentally safe membranes for water remediation and desalination applications.

■ ASSOCIATED CONTENT

Supporting Information

The Supporting Information is available free of charge on the ACS Publications website at DOI: 10.1021/acsami.8b20598.

Characterization of $Mg(OH)_2$, GQDs, forward osmosis setup, AFM height profile, long-term stability studies, XRD of dry and wet GO membranes, and calculation of *d*-spacings (PDF)

■ AUTHOR INFORMATION

Corresponding Author

*E-mail: sbose@iisc.ac.in. Tel.: +91-80-22933407.

ORCID

Shabnam Pathan: 0000-0002-5869-0150

Suryasarathi Bose: 0000-0001-8043-9192

Notes

The authors declare no competing financial interest.

■ ACKNOWLEDGMENTS

This work is supported by the Department of Science and Technology (DST), India, and the authors N.P., L.D.G., and S.P. acknowledge DST Young Scientist fellowships and Women Scientist-B fellowship for their funding (YSS/2014/000165, YSS/2015/001448, and SR/WOS-B/565/2016, respectively). The authors further acknowledge the characterization support from CeNSE.

■ REFERENCES

(1) Shannon, M. A.; Bohn, P. W.; Elimelech, M.; Georgiadis, J. G.; Mariñas, B. J.; Mayes, A. M. Science and technology for water purification in the coming decades. *Nature* **2008**, *452*, 301−310.

(2) An, D.; Yang, L.; Wang, T.-J.; Liu, B. Separation Performance of Graphene Oxide Membrane in Aqueous Solution. *Ind. Eng. Chem. Res.* **2016**, 4803−4810.

(3) Sreeprasad, T.; Maliyekkal, S. M.; Lisha, K.; Pradeep, T. Reduced graphene oxide−metal/metal oxide composites: facile synthesis and application in water purification. *J. Hazard. Mater.* **2011**, *186*, 921−931.

(4) Hegab, H. M.; Zou, L. Graphene oxide-assisted membranes: fabrication and potential applications in desalination and water purification. *J. Membr. Sci.* **2015**, *484*, 95−106.

(5) Zheng, S.; Tu, Q.; Urban, J. J.; Li, S.; Mi, B. Swelling of Graphene Oxide Membranes in Aqueous Solution: Characterization of Interlayer Spacing and Insight into Water Transport Mechanisms. *ACS Nano* **2017**, 6440−6450.

(6) Lim, M.-Y.; Choi, Y.-S.; Kim, J.; Kim, K.; Shin, H.; Kim, J.-J.; Shin, D. M.; Lee, J.-C. Cross-linked graphene oxide membrane having high ion selectivity and antibacterial activity prepared using tannic acid-functionalized graphene oxide and polyethyleneimine. *J. Membr. Sci.* **2017**, *521*, 1−9.

(7) Fei, F.; Cseri, L.; Szekely, G.; Blanford, C. F. Robust Covalently Cross-linked Polybenzimidazole/Graphene Oxide Membranes for High-Flux Organic Solvent Nanofiltration. *ACS Appl. Mater. Interfaces* **2018**, *10*, 16140−16147.

(8) Li, W.; Wu, W.; Li, Z. Controlling Interlayer Spacing of Graphene Oxide Membranes by External Pressure Regulation. *ACS Nano* **2018**, *12*, 9309−9317.

(9) Thebo, K. H.; Qian, X.; Zhang, Q.; Chen, L.; Cheng, H.-M.; Ren, W. Highly stable graphene-oxide-based membranes with superior permeability. *Nat. Commun.* **2018**, No. 1486.

(10) Liu, Q.; Gupta, K. M.; Xu, Q.; Liu, G.; Jin, W. Gas permeation through double-layer graphene oxide membranes: The role of interlayer distance and pore offset. *Sep. Purif. Technol.* **2019**, *209*, 419−425.

(11) Devanathan, R.; Chase-Woods, D.; Shin, Y.; Gotthold, D. W. Molecular Dynamics Simulations Reveal that Water Diffusion between Graphene Oxide Layers is Slow. *Sci. Rep.* **2016**, *6*, No. 29484.

(12) Chen, L.; Shi, G.; Shen, J.; Peng, B.; Zhang, B.; Wang, Y.; Bian, F.; Wang, J.; Li, D.; Qian, Z.; Xu, G.; Liu, G.; Zeng, J.; Zhang, L.; Yang, Y.; Zhou, G.; Wu, M.; Jin, W.; Li, J.; Fang, H. Ion sieving in graphene oxide membranes via cationic control of interlayer spacing. *Nature* **2017**, *550*, 380−383.

(13) Abraham, J.; Vasu, K. S.; Williams, C.; Gopinadhan, K.; Su, Y.; Cherian, C.; Dix, J.; Prestat, E.; Haigh, S.; Grigorieva, I.; Carbone, P.; K Geim, A.; Raveendran-Nair, R. Tuneable Sieving of Ions Using Graphene Oxide Membranes. *Nat. Nanotechnol.* **2017**, *12*, 546−550.

(14) Lin, X.; Shen, X.; Sun, X.; Liu, X.; Wu, Y.; Wang, Z.; Kim, J.-K. Graphene Oxide Papers Simultaneously Doped with Mg2+ and Cl− for Exceptional Mechanical, Electrical, and Dielectric Properties. *ACS Appl. Mater. Interfaces* **2016**, *8*, 2360−2371.

(15) Zhang, C.; Wei, K.; Zhang, W.; Bai, Y.; Sun, Y.; Gu, J. Graphene Oxide Quantum Dots Incorporated into a Thin Film Nanocomposite Membrane with High Flux and Antifouling Properties for Low-Pressure Nanofiltration. *ACS Appl. Mater. Interfaces* **2017**, *9*, 11082−11094.

(16) Padmavathy, N.; Jaidev, L. R.; Bose, S.; Chatterjee, K. Oligomer-grafted graphene in a soft nanocomposite augments mechanical properties and biological activity. *Mater. Des.* **2017**, *126*, 238−249.

(17) Wang, Q.; Li, C.; Guo, M.; Sun, L.; Hu, C. Hydrothermal synthesis of hexagonal magnesium hydroxide nanoflakes. *Mater. Res. Bull.* **2014**, *51*, 35−39.

(18) Lu, Q.; Wu, C.; Liu, D.; Wang, H.; Su, W.; Li, H.; Zhang, Y.; Yao, S. A facile and simple method for synthesis of graphene oxide quantum dots from black carbon. *Green Chem.* **2017**, *19*, 900−904.

(19) Jia, Z.; Wang, Y. Covalently crosslinked graphene oxide membranes by esterification reactions for ions separation. *J. Mater. Chem. A* **2015**, *3*, 4405−4412.
(20) Yang, Q.; Wang, K. Y.; Chung, T.-S. Dual-Layer Hollow Fibers with Enhanced Flux As Novel Forward Osmosis Membranes for Water Production. *Environ. Sci. Technol.* **2009**, *43*, 2800−2805.
(21) Padmavathy, N.; Samantaray, P. K.; Ghosh, L. D.; Madras, G.; Bose, S. Selective cleavage of the polyphosphoester in crosslinked copper based nanogels: enhanced antibacterial performance through controlled release of copper. *Nanoscale* **2017**, *9*, 12664−12676.
(22) Park, S.; Lee, K.-S.; Bozoklu, G.; Cai, W.; Nguyen, S. T.; Ruoff, R. S. Graphene Oxide Papers Modified by Divalent Ions—Enhancing Mechanical Properties via Chemical Cross-Linking. *ACS Nano* **2008**, *2*, 572−578.
(23) Koltonow, A. R.; Luo, C.; Luo, J.; Huang, J. Graphene Oxide Sheets in Solvents: To Crumple or Not To Crumple? *ACS Omega* **2017**, *2*, 8005−8009.
(24) Sun, Y.; Wang, S.; Li, C.; Luo, P.; Tao, L.; Wei, Y.; Shi, G. Large scale preparation of graphene quantum dots from graphite with tunable fluorescence properties. *Phys. Chem. Chem. Phys.* **2013**, *15*, 9907−9913.
(25) Yu, W.; Tong, Y.; Nigel, G. Development of a stable cation modified graphene oxide membrane for water treatment. *2D Mater.* **2017**, *4*, No. 045006.
(26) Fromm, K. M. Coordination polymer networks with s-block metal ions. *Coord. Chem. Rev.* **2008**, *252*, 856−885.
(27) Abolhassani, M.; Griggs, C. S.; Gurtowski, L. A.; Mattei-Sosa, J. A.; Nevins, M.; Medina, V. F.; Morgan, T. A.; Greenlee, L. F. Scalable Chitosan-Graphene Oxide Membranes: The Effect of GO Size on Properties and Cross-Flow Filtration Performance. *ACS Omega* **2017**, *2*, 8751−8759.
(28) Huang, Z.; Rajasekaran, P.; Ozcan, A.; Santra, S. Antimicrobial Magnesium Hydroxide Nanoparticles As an Alternative to Cu Biocide for Crop Protection. *J. Agric. Food Chem.* **2018**, *66*, 8679−8686.
(29) Akhavan, O.; Ghaderi, E. Toxicity of Graphene and Graphene Oxide Nanowalls Against Bacteria. *ACS Nano* **2010**, *4*, 5731−5736.
(30) Liu, S.; Hu, M.; Zeng, T. H.; Wu, R.; Jiang, R.; Wei, J.; Wang, L.; Kong, J.; Chen, Y. Lateral dimension-dependent antibacterial activity of graphene oxide sheets. *Langmuir* **2012**, *28*, 12364−12372.
(31) Zou, F.; Zhou, H.; Jeong, D. Y.; Kwon, J.; Eom, S. U.; Park, T. J.; Hong, S. W.; Lee, J. Wrinkled Surface-Mediated Antibacterial Activity of Graphene Oxide Nanosheets. *ACS Appl. Mater. Interfaces* **2017**, *9*, 1343−1351.
(32) Liu, S.; Zeng, T. H.; Hofmann, M.; Burcombe, E.; Wei, J.; Jiang, R.; Kong, J.; Chen, Y. Antibacterial Activity of Graphite, Graphite Oxide, Graphene Oxide, and Reduced Graphene Oxide: Membrane and Oxidative Stress. *ACS Nano* **2011**, *5*, 6971−6980.
(33) Samantaray, P. K.; Madras, G.; Bose, S. PVDF/PBSA membranes with strongly coupled phosphonium derivatives and graphene oxide on the surface towards antibacterial and antifouling activities. *J. Membr. Sci.* **2018**, *548*, 203−214.
(34) Szunerits, S.; Boukherroub, R. Antibacterial activity of graphene-based materials. *J. Mater. Chem. B* **2016**, *4*, 6892−6912.
(35) Dreyer, D. R.; Park, S.; Bielawski, C. W.; Ruoff, R. S. The chemistry of graphene oxide. *Chem. Soc. Rev.* **2010**, *39*, 228−240.
(36) Homaeigohar, S.; Elbahri, M. Graphene membranes for water desalination. *NPG Asia Mater.* **2017**, *9*, No. e427.
(37) Han, J.-L.; Xia, X.; Haider, M. R.; Jiang, W.-L.; Tao, Y.; Liu, M.-J.; Wang, H.-c.; Ding, Y.-C.; Hou, Y.-N.; Cheng, H.-Y.; Wang, A.-J. Functional graphene oxide membrane preparation for organics/inorganic salts mixture separation aiming at advanced treatment of refractory wastewater. *Sci. Total Environ.* **2018**, *628−629*, 261−270.
(38) Qu, G.; Wang, X.; Wang, Z.; Liu, S.; Jiang, G. Cytotoxicity of quantum dots and graphene oxide to erythroid cells and macrophages. *Nanoscale Res. Lett.* **2013**, *8*, No. 198.
(39) Wu, C.; Chong, W.; Ting, H.; Xuejiao, Z.; Shouwu, G.; Jingyan, Z. Insight into the Cellular Internalization and Cytotoxicity of Graphene Quantum Dots. *Adv. Healthcare Mater.* **2013**, *2*, 1613−1619.

DOI: 10.1021/acsami.8b20598
ACS Appl. Mater. Interfaces 2019, 11, 7566−7575